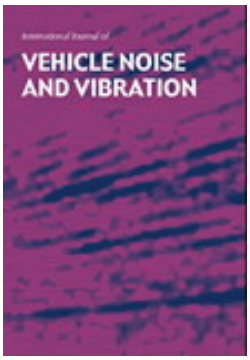

International Journal of Vehicle Noise and Vibration

ISSN online: 1479-148X - ISSN print: 1479-1471
https://www.inderscience.com/ijvnv

Stator vibration analysis of in-wheel motor for electric vehicle based on harmonic response analysis method

Qiping Chen, Xuanjun Huang, Hao Shao, Junling Ding, Zhihui Xu

DOI: 10.1504/IJVNV.2022.10050579

Article History:
Received: 02 April 2021
Accepted: 16 December 2021
Published online: 16 September 2022

Stator vibration analysis of in-wheel motor for electric vehicle based on harmonic response analysis method

Qiping Chen*, Xuanjun Huang and Hao Shao

Key Laboratory of Vehicle and Equipment,
Ministry of Education,
East China Jiaotong University,
Nanchang 330013, China
and
Nanchang Key Laboratory of New Energy Vehicles,
East China Jiaotong University,
Nanchang 330013, China
Fax: +86-791-87046108
Email: qiping3846758@163.com
Email: 1055132617@qq.com
Email: 1429093339@qq.com
*Corresponding author

Junling Ding

Key Laboratory of Vehicle and Equipment,
Ministry of Education,
East China Jiaotong University,
Nanchang 330013, China
Email: 2276327532@qq.com

Zhihui Xu

Key Laboratory of Vehicle and Equipment,
Ministry of Education,
East China Jiaotong University,
Nanchang 330013, China
and
Nanchang Key Laboratory of New Energy Vehicles,
East China Jiaotong University,
Nanchang 330013, China
Email: 519260146@qq.com

Abstract: In order to effectively reduce the vibration and noise of in-wheel motor for electric vehicle, the radial electromagnetic force wave of in-wheel motor under load is decomposed by Fourier transform, and the results are obtained. The radial electromagnetic force wave has large harmonic amplitude and wide frequency distribution. Finally, the free mode and harmonic response of three different stator configurations are analysed. The results show that: under the action of the radial force wave, the maximum deformation of the stator without cooling channel is 6.639e–5 mm, the maximum deformation of

the stator with radial cooling channel is 5.8224e–5 mm, and the maximum deformation of the stator with axial cooling channel is 6.864e–5 mm. The deformation is very small, and there will be no friction and collision between the stator and the rotor during the operation of the in-wheel motor.

Keywords: electric vehicle; in-wheel motor; radial force wave; harmonic vibration.

Reference to this paper should be made as follows: Chen, Q., Huang, X., Shao, H., Ding, J. and Xu, Z. (2022) 'Stator vibration analysis of in-wheel motor for electric vehicle based on harmonic response analysis method', *Int. J. Vehicle Noise and Vibration*, Vol. 18, Nos. 1/2, pp.61–76.

Biographical notes: Qiping Chen received his PhD in Mechanical Engineering from the Chongqing University, Chongqing, China, in 2013. He is currently an Associate Professor of the School of Mechanical Electronic and Vehicle Engineering, East China Jiaotong University, China. His research interests include electric vehicles, hybrid vehicles, mechatronics, etc.

Xuanjun Huang is currently an MS student in the School of Mechanical Electronic and Vehicle Engineering, East China Jiaotong University, China. His research interests include electric vehicles, vehicle dynamics, mechatronics, etc.

Hao Shao is currently an MS student in the School of Mechanical Electronic and Vehicle Engineering, East China Jiaotong University, China. His research interests include electric vehicles, vehicle dynamics, mechatronics, etc.

Junling Ding is currently holds a PhD in the School of Mechanical Electronic and Vehicle Engineering, East China Jiaotong University, China. His research interests include electric vehicles, vehicle dynamics, mechatronics, etc.

Zhihui Xu is currently an MS student in the School of Mechanical Electronic and Vehicle Engineering, East China Jiaotong University, China. His research interests include electric vehicles, vehicle dynamics, mechatronics, etc.

1 Introduction

1.1 Writing motivation and current challenges

Energy crisis and environmental pollution are becoming more and more serious (Chen et al., 2019, 2021). The development of electric vehicles has attracted the attention of all countries in the world. It is of great significance to carry out the research on electric vehicles. In-wheel motor is one of the core components of electric vehicle drive system (Wu et al., 2013), and its vibration and noise will affect the performance of in-wheel motor (Sun et al., 2015). As the electromagnetic force acts directly on the stator tooth end and magnetic pole of in-wheel motor, the electromagnetic noise mainly comes from the vibration of stator yoke. In the case of the same sound pressure level, the noise of the in-wheel motor has more subjective influence on the driver than that of the engine noise, which further affects the driver's comfort. Therefore, this paper takes the permanent

magnet brushless in-wheel motor as the research object, and analyses the radial force wave and vibration deformation of the stator.

1.2 Literature review

Zhang et al. (2019) verified the resonance range of the in-wheel motor through sound pressure experiment and impedance experiment, and optimised the structure of the in-wheel motor, but lacked the analysis of the radial force wave. Zhan et al. (2019) of Wuhan Marine Electric Propulsion Research Institute analysed the radial air gap flux density and radial electromagnetic force wave of surface mounted permanent magnet synchronous motor under straight slot and inclined slot, which showed that inclined slot could reduce the amplitude of low order exciting force, but the research on stator shape was lacking. Lin et al. (2016) used Fourier transform and finite element method to calculate the frequency of force components in a specific spatial order, and found that the influence of current harmonics on vibration and noise depends on their influence on the lowest spatial order force, but did not give the corresponding optimisation scheme. Dong et al. (2019) proposed a rotor step model that can affect the electromagnetic interference, which can predict and suppress the electromagnetic vibration and noise of electric vehicle drive motor, but lacked of experimental verification. Hara et al. (2017) used the coupling analysis of circuit simulator and two-dimensional finite element analysis (2D FEM) to study the electromagnetic force producing noise, and showed that the electromagnetic noise and vibration are caused by the 0 order electromagnetic force of spatial harmonics, but lacked relevant theoretical analysis. Jiang et al. (2020) analysed the vibration characteristics of the stator by using the finite element method, and measured the resonance frequency and radial vibration amplitude of the stator by using the laser vibration meter. The measured results are consistent with the theoretical analysis results. Pezzaniab et al. (2017) proposed a resampling technique based on sequential tracking without measuring rotor position to detect the vibration of in-wheel motor, but the simulation process is too simple. Lin et al. (2018) studied the influence of rotor eccentricity on the vibration and noise of in-wheel motor, and determined that the peak value of vibration and noise would transfer to the frequency band near the low modal frequency. Wang and Li (2020) proposed an improved rotor structure with an auxiliary flux barrier to reduce the radial electromagnetic force, so as to reduce the electromagnetic vibration and noise. The simulation and experimental results prove the effectiveness and validity of the design (Wang and Li, 2020). Lu et al. (2020) calculated the influence of broken bar fault on the vibration and noise of in-wheel motor through multi physical field simulation, and the simulation and experiment are highly consistent. Wang et al. (2019) optimised the vibration and noise of the in-wheel motor for the NVH problem, and verified the effectiveness through experiments, but the formula derivation is slightly insufficient. Through the vibration detection and analysis of permanent magnet DC motor, Liang et al. (2014) proved that the motor vibration experimental system composed of computer and LabVIEW can fully meet the requirements of in-wheel motor test and fault classification research. Jing and Cheng (2019) proposed a new type of rotor profile to reduce the ripple torque of switched reluctance motor. Through simulation analysis, the structure can significantly reduce the ripple torque of in-wheel motor (Jing and Cheng, 2019).

1.3 Scientific and engineering contributions

The vibration and noise problem of in-wheel motor has been one of the core reasons restricting the development of electric vehicle drive system. According to the analysis of the above literature, scholars put forward various solutions to the problems of electromagnetic force wave and harmonic vibration, such as changing the magnetic pole structure, optimising the stator structure and so on. Therefore, based on previous studies, this paper analyses the influence of radial force wave on vibration in detail, and makes three contributions:

1 revealing the generation mechanism of radial force wave

2 analysing the vibration and deformation of different stator structures of in-wheel motor

3 proposing a harmonic response analysis method of in-wheel motor stator.

1.4 Article organisation structure

In this paper, aiming at the vibration and noise problems of the in-wheel motor, firstly, the calculation formula of the radial force wave of the in-wheel motor is derived; secondly, the radial electromagnetic force wave of the in-wheel motor is decomposed by Fourier transform; finally, the modal and harmonic responses of the stator with three different structures are analysed.

2 Calculation of radial force wave

According to Maxwell tensor method, the formula for calculating the stress density generated by the magnetic field strength between the object and its surface in vacuum is shown in formula (1) (Gao et al., 2019).

$$P_f = \frac{1}{2}\mu_0 H^2 \tag{1}$$

Here: P_f is the electromagnetic force density acting on the surface of the object, μ_0 is the vacuum permeability, and H is the intensity of the magnetic field.

When the in-wheel motor is running, the direction of some magnetic lines of force is curved, so the magnetic field intensity in the air gap is also curved. According to Maxwell tensor method, the magnetic pull density generated in the air gap can be decomposed into radial electromagnetic force density and tangential electromagnetic force density, and the calculation formula is shown in formula (2).

$$\begin{cases} P_r = \dfrac{B_r^2 - B_t^2}{2\mu_0} \\ P_t = \dfrac{B_r B_t}{\mu_0} \end{cases} \tag{2}$$

Here: P_r is the radial force density of in-wheel motor, P_t is the tangential electromagnetic force of in-wheel motor, B_r is the radial flux density of in-wheel motor, and B_t is the tangential flux density of the in-wheel motor.

For in-wheel motor, B_r is larger than B_t. In order to simplify the calculation and ignore the influence of tangential air gap flux density, the radial electromagnetic force density is simplified as formula (3).

$$p_r \approx \frac{B_r^2}{2\mu_0}. \tag{3}$$

2.1 Calculation of radial electromagnetic force of in-wheel motor under no-load

According to Maxwell tensor method, the electromagnetic force of in-wheel motor under no-load condition is analysed. When the in-wheel motor is no-load, the current in the armature winding can be ignored, and when it is no-load, the permanent magnet provides the magnetic field. The magnetic field provided by the permanent magnet enters the stator part of the in-wheel motor through the air gap, and then enters the rotor through the air gap to form a closed magnetic circuit. According to formula (3), in order to obtain the radial electromagnetic force of the in-wheel motor under no-load condition, it is necessary to obtain the radial air gap magnetic density distribution of the in-wheel motor. Generally, the magnetic potential multiplication method is used to solve the problem. According to the magnetic potential multiplication method (Wang and Qiu, 2012), the air gap magnetic density of in-wheel motor is calculated, as shown in formula (4).

$$b(\theta, t) = F(\theta, t)\Lambda(\theta, t) \tag{4}$$

Here: $F(\theta, t)$ is distribution function of magnetic potential and $\Lambda(\theta, t)$ is air gap permeability.

When the in-wheel motor has no-load, the air gap magnetic potential is only generated by the permanent magnet. The Fourier decomposition of the magnetic potential generated by the permanent magnet can be obtained, as shown in formula (5).

$$F(\theta, t) = \sum_{\mu} F_\mu \cos \omega_\mu - \mu\theta \tag{5}$$

Here: μ is the order of harmonics, F_μ is the harmonic amplitude and ω_μ is harmonic angular velocity.

Considering the smooth slotted stator and rotor, the air gap permeability is as follows:

$$\Lambda(\theta, t) = \Lambda_0 + \sum_{k=1}^{\infty} \Lambda_k \cos kZ_1\theta \tag{6}$$

Here: Λ_0 is the average air gap permeability amplitude, k is the number of k of air gap permeability amplitudes caused by stator slots is calculated and Z_1 is the number of stator slots.

By substituting formula (5) and formula (6) into formula (4), the radial air gap magnetic density distribution of permanent magnet material under no-load is obtained, as shown in formula (7).

$$b_m(\theta,t)=\sum_{\mu}F_{\mu}\Lambda_0\cos\left(\mu\frac{\omega}{p}t-\mu\theta\right)+\sum_{\mu}\sum_{k}(-1)^{k+1}\frac{1}{2}B_{\mu}\Lambda_k\cos\left[\mu\frac{\omega}{p}t-\mu\pm kZ_1\theta\right] \quad (7)$$

By substituting formula (7) into formula (3), the distribution expression of radial electromagnetic force is as follows:

$$\begin{aligned}
p_r(\theta,t)&=\frac{1}{2\mu_0}\left\{\sum_{\mu}F_{\mu}\Lambda_0\cos\left(\mu\frac{\omega_1}{p}t-\mu\theta\right)\right.\\
&\left.+\frac{1}{2}\sum_{\mu}\sum_{k}(-1)^{k+1}F_{\mu}\Lambda_k\cos\left[\mu\frac{\omega_1}{p}t-\mu\pm kZ_1\theta\right]\right\}^2\\
&=\sum_{\mu}\frac{1}{4\mu_0}F_{\mu}\Lambda_0^2+\sum_{\mu}\sum_{k}\frac{1}{16\mu_0}F_{\mu}\Lambda_k^2+\sum_{\mu}\frac{1}{4\mu_0}F_{\mu}\Lambda_0^2\cos\left(2\mu\frac{\omega_l}{p}t-2\mu\theta\right)\\
&+\sum_{\mu}\sum_{k}\frac{1}{16\mu_0}F_{\mu}\Lambda_k^2\cos\left[2\mu\frac{\omega_1}{p}t-2\mu\pm kZ_1\theta\right]\\
&+\sum_{\mu_1}\sum_{\mu_2}\frac{1}{2\mu_0}F_{\mu}F_{\mu_2}\Lambda_0^2\cos\left[(\mu_1\pm\mu_2)\frac{\omega_1}{p}t-(\mu_1\pm\mu_2)\theta\right],\ \mu_1>\mu_2\\
&+\sum_{\mu}\sum_{\mu_k}\sum_{k_1}\sum_{k_2}(-1)^{k_1+k_2}\frac{1}{8\mu}F_{\mu_1}F_{\mu_2}\Lambda_{k_1}\Lambda_{k_2}\cos\left\{(\mu_1\pm\mu_2)\frac{\omega_1}{p}t\right.\\
&\left.-\left[(\mu_1\pm\mu_2)\pm(k_2\pm k_1)Z_1\right]\theta\right\}(\mu_2>\mu_1,k_2>k_1)\\
&+\sum_{\mu}\sum_{\mu_2}\sum_{k}(-1)^{k+1}\frac{1}{4\mu_0}F_{\mu_1}F_{\mu_2}\Lambda_{k_1}\Lambda_{k_2}\cos\left\{(\mu_1\pm\mu_2)\frac{\omega_1}{p}t-\left[(\mu_2\pm\mu_1)\pm kZ_1\right]\theta\right\}
\end{aligned} \quad (8)$$

According to formula (8), no-load can be divided into six radial electromagnetic force components, as shown in Table 1

Table 1 Source and function of no-load radial electromagnetic force

Radial force wave	*Source*	*Effect*
(1)	Interaction between harmonic and permeance of permanent magnet	It does not cause vibration, therefore, it is generally not studied
(2) (3)	Electromagnetic force of fundamental component acting on itself	The frequency of this part of the electromagnetic force will be far away from the lowest natural frequency of the in-wheel motor stator to avoid resonance
(4) (5) (6)	Electromagnetic force wave generated by interaction of different harmonics of permanent magnet	It contains low order harmonic and high order harmonic, which is the main part of weakening radial electromagnetic force of in-wheel motor

2.2 Calculation of radial electromagnetic force of in-wheel motor under load

When the in-wheel motor is loaded, the air gap magnetic field is produced by the interaction of permanent magnet and armature winding. When the current passes through the winding, the air gap magnetic density distribution generated by the armature winding is shown in formula (9) (Verez et al., 2015).

$$b_w(\theta, t) = \sum_v B_v \cos[\omega_1 t - v\theta - \varphi] \tag{9}$$

Here: φ is the angle between the winding and the magnetic field axis of the permanent magnet and v is the harmonic order of the winding magnetic field.

Therefore, under the action of load, the radial electromagnetic force per unit area is:

$$P_n = \frac{[b_m(\theta, t) + b_n(\theta, t)]^2}{2\mu_0} \tag{10}$$

Expand and decompose formula (10). In addition to the no-load radial electromagnetic force wave as shown in formula (8), the new radial electromagnetic force wave introduced by armature winding can be divided into the following five parts, as shown in Table 2:

$$\begin{aligned}
&(1)\ \sum_v \frac{1}{4\mu_0} B_v^2 + \sum_{v_1}\sum_{v_2} \frac{1}{2\mu_0} B_{v_1} B_{v_2} \cos[v_2 - v_1\theta],\ v_2 > v_1 \\
&(2)\ \sum_v \frac{1}{4\mu_0} B_v^2 \cos[2\omega_1 t - 2v\theta - 2\phi] \\
&(3)\ \sum_{v_1}\sum_{v_2} \frac{1}{2\mu_0} B_{v_1} B_{v_2} \cos[2\omega t - v_2 + v_1\theta - 2\phi],\ v_2 > v_1 \\
&(4)\ \sum_v \sum_\mu \frac{1}{2\mu_0} B_v F_\mu \Lambda_0 \cos\left[(\mu \pm p)\frac{\omega_1}{p} t - (\mu \pm v)\theta \pm \phi\right] \\
&(5)\ \sum_v \sum_\mu \sum_k (-1)^{k+1} \frac{1}{4\mu_0} B_v F_\mu \Lambda_k \cos\left[(\mu \pm p)\frac{\omega_1}{p} t - [\mu \pm kZ_1 \pm v\theta] \pm \phi\right]
\end{aligned} \tag{11}$$

Table 2 Source and function of radial electromagnetic force of load

Radial force wave	*Source*	*Effect*
(1)	Electromagnetic force wave produced by magnetic field of armature winding and its own action	The main weakening part of electromagnetic force
(2)		
(3)		
(4)	The electromagnetic force generated by the interaction of stator armature magnetic field, rotor permanent magnet magnetic field and air gap permeance	Basically no impact
(5)		

For mechanical vibration, the peak value of vibration amplitude is inversely proportional to the fourth power of force wave order:

$$\xi_{\max} \propto \frac{\omega\left(\frac{L}{4m}\right)^2}{E\rho L R_o^4 - R_i^4}\left(\frac{L}{2m} - \frac{L}{4m}\right) \propto \frac{\omega}{R_o^4 - R_i^4}\frac{1}{m^4} \tag{12}$$

Here: $\xi_{\max}$ is the maximum displacement of mechanical structure, E is the Young's modulus of the material, ρ is the density of the material, L is the axial length of the stator, m is the order of force wave, R_o and R_i are the inner diameter and outer diameter of cylindrical shell, respectively.

It can be seen from formula (12) that if the electromagnetic force amplitudes of low-order force wave and high-order force wave is the same, the vibration amplitude caused by low-order force wave is greater than that caused by high-order force wave. Therefore, in the electromagnetic design, it is necessary to optimise and weaken the low-order electromagnetic force wave in the in-wheel motor.

3 Simulation experiment analysis

3.1 Radial force wave analysis

The model used in this paper is a permanent magnet brushless DC in-wheel motor. The parameters of the selected in-wheel motor are shown in Table 3.

Table 3 Basic parameters of in-wheel motor

Project	*Parameter*	*Project*	*Parameter*
Rated power (kw)	12	Rated voltage (V)	310
Phase number	3	Number of slots	24
Stator outer diameter (mm)	306.4	Stator inner diameter (mm)	125
Rotor outer diameter (mm)	343	Rotor inner diameter (mm)	310
Thickness of permanent magnet (mm)	5	Magnetic steel type	NdFe35
Polar arc coefficient	0.5	Stacking coefficient	0.95
Axial length (mm)	48	Stator slot shape	Pear shaped groove

According to the above parameters, the 2D model is established in Maxwell, and the material, excitation and boundary conditions are setup. Because the mesh division of air gap between stator and rotor is closely related to the accuracy of solving radial force wave, the air gap is divided into six layers, and the minimum mesh size of each layer is set to 1 mm. The amplitude and frequency distribution of radial electromagnetic force wave of in-wheel motor are simulated and analysed by finite element software. The radial air gap flux density and radial electromagnetic force wave distribution of in-wheel motor under load can be obtained, as shown in Figure 1 and Figure 2. It can be seen from Figure 1 and Figure 2 that the air gap flux density of in-wheel motor contains more harmonic components, and the fundamental wave amplitude is about 1.2 T. The

interaction between harmonics and harmonics, harmonics and fundamental wave will produce many radial electromagnetic force waves with different frequencies and amplitudes, which will cause the vibration of in-wheel motor at various frequencies. In particular, the greater amplitude of radial electromagnetic force generated by the interaction between harmonics and fundamental wave will cause greater vibration. From the trend of Figure 1 and Figure 2, the air gap flux density and radial force wave follow a certain sine trend and present a certain rule, but the trend of radial force wave is more disordered and there are more burrs, which will have a significant effect on the vibration of in-wheel motor. The Fourier decomposition (FFT) of the radial electromagnetic force wave of the in-wheel motor under load is obtained as shown in Figure 3. It can be seen from Figure 3 that the radial electromagnetic force generated by the in-wheel motor has large harmonic amplitude and wide frequency distribution, which is easier to cause the resonance of the in-wheel motor structure and increase the vibration amplitude of the in-wheel motor.

Figure 1 Radial air gap flux density of in-wheel motor, (a) time distribution of single point radial magnetic density (b) circumferential radial magnetic density distribution (see online version for colours)

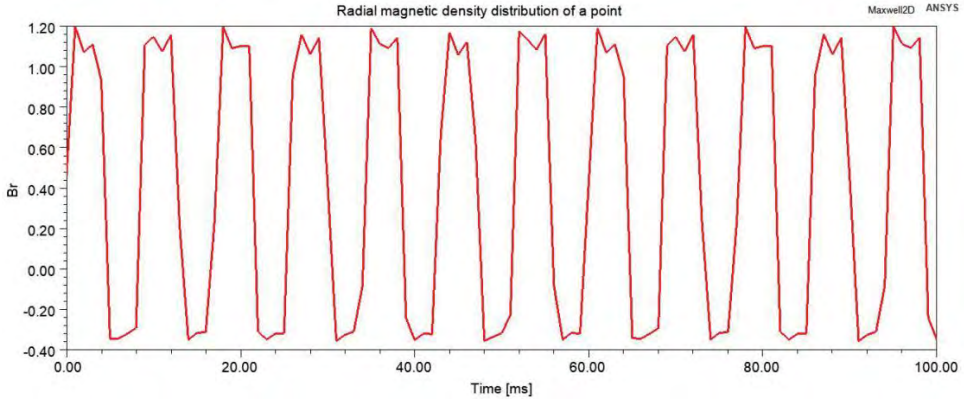

(a)

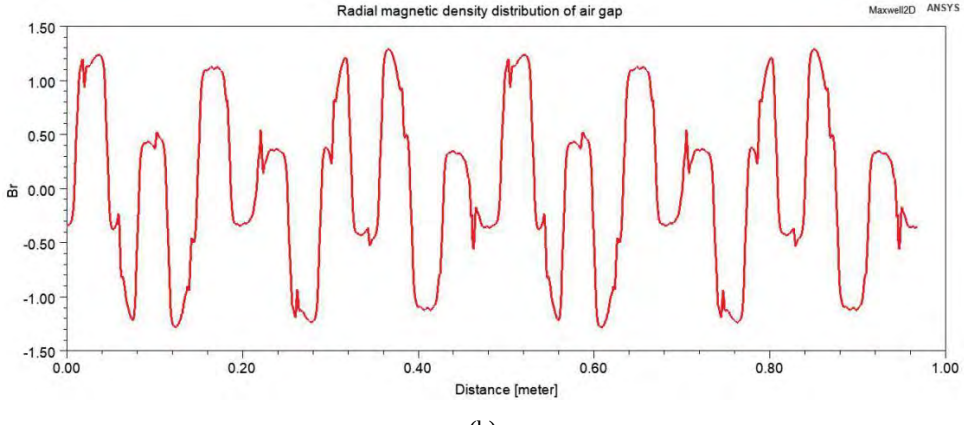

(b)

Figure 2 Air gap radial force wave of in-wheel motor, (a) time distribution of radial force at a single point (b) circumferential radial force distribution (see online version for colours)

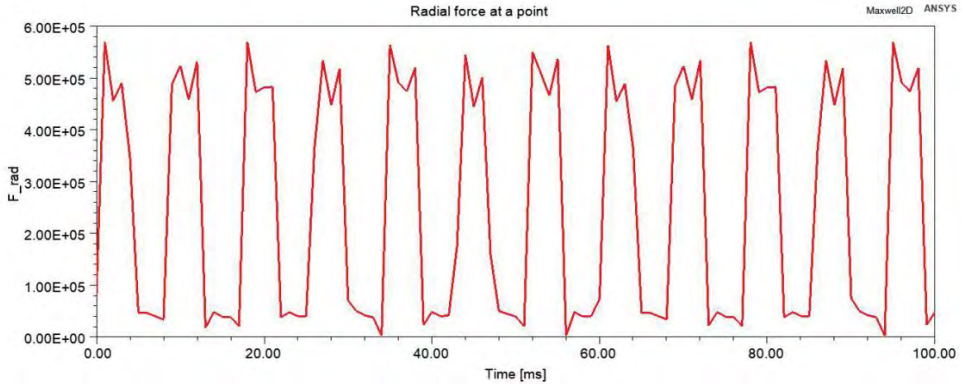

(a)

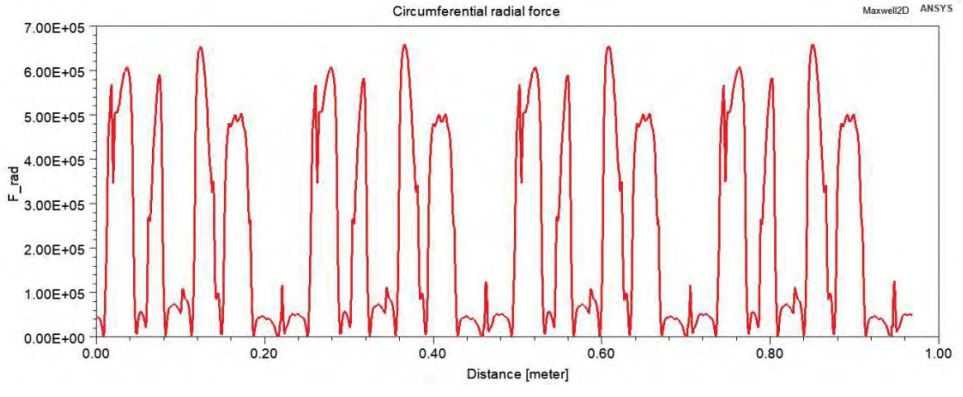

(b)

3.2 Vibration analysis

It can be seen from the above analysis that the vibration of in-wheel motor is mainly due to the effect of electromagnetic force, especially the effect of radial force wave on stator and rotor. But the final form of vibration is shown in the mechanical structure, mechanical vibration will produce deformation and noise, so it is very necessary to carry out modal analysis on the mechanical structure. In this paper, the free modal analysis of three different stator shapes is carried out.

Figure 4 shows three kinds of stator structures, among which Figure 4(a) shows the stator structure without cooling channel, Figure 4(b) shows the stator structure with radial cooling channel, and Figure 4(c) shows the stator structure with axial cooling channel. Figure 5 shows the modes of the three stator structures. It can be seen from Figure 5 that in the case of free mode analysis, the first six modal frequencies of the stator structure with 6 degrees of freedom are basically 0; from the seventh modal, the higher the natural frequencies are; from the frequencies of the three stator structures with the same modal, the influence of cooling channels on the natural frequencies is basically small, but the natural frequencies of the radial channels are small. It will be a little higher.

Figure 3 Fourier decomposition of air gap radial force wave of in-wheel motor, (a) single point Fourier decomposition (b) circular Fourier decomposition (see online version for colours)

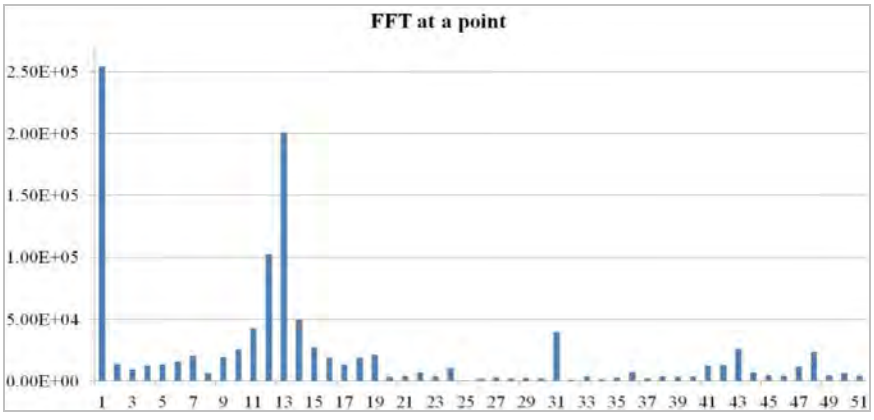

(a)

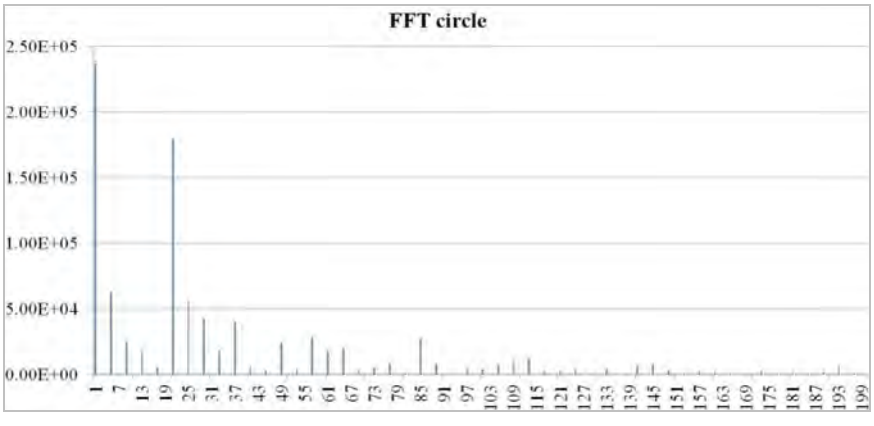

(b)

In ANSYS finite element software, the harmonic responses of three kinds of stator structures are analysed respectively. Among them, Figure 5(a) is the harmonic response result of the stator without cooling channel, Figure 5(b) is the harmonic response result of the stator with radial cooling channel, and Figure 5(c) is the harmonic response result of the stator with axial cooling channel. It can be seen from Figure 6 that under the action of radial force wave, the maximum deformation of the stator without cooling channel is 6.639e–5 mm, the maximum deformation of the stator with radial cooling channel is 5.8224e–5 mm, and the maximum deformation of the stator with axial cooling channel is 6.864e–5 mm. The deformation is very small, and there will be no friction and collision between the stator and the rotor during the operation of the in-wheel motor. In the structure, the stator deformation of the axial cooling channel is the largest, so it can be considered to optimise the structure of the axial cooling channel in the research and development process of the in-wheel motor, so as to reduce the deformation in the vibration process. But in general, the three stator structures will not affect the normal operation of in-wheel motor under the action of radial force wave.

Figure 4 Three stator structures, (a) stator structure without cooling channel (b) stator structure of radial cooling channel (c) stator structure of axial cooling channel (see online version for colours)

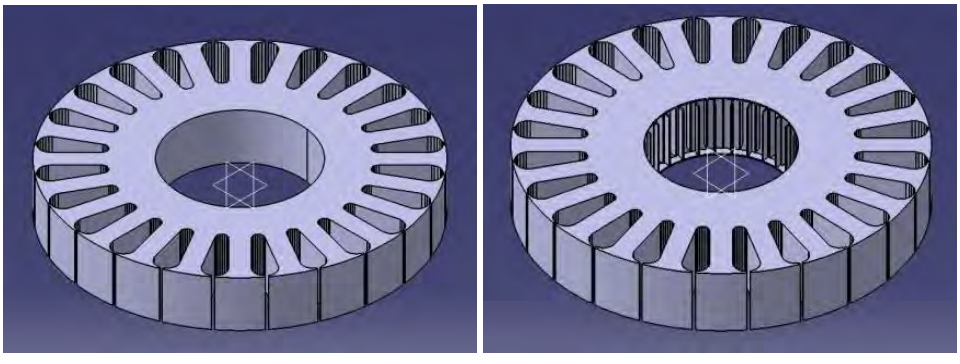

(a) (b)

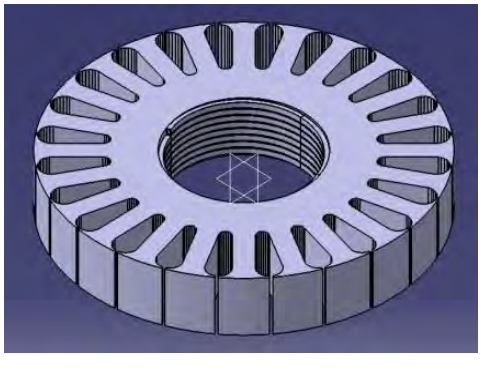

(c)

Figure 5 Modes of three stator structures (see online version for colours)

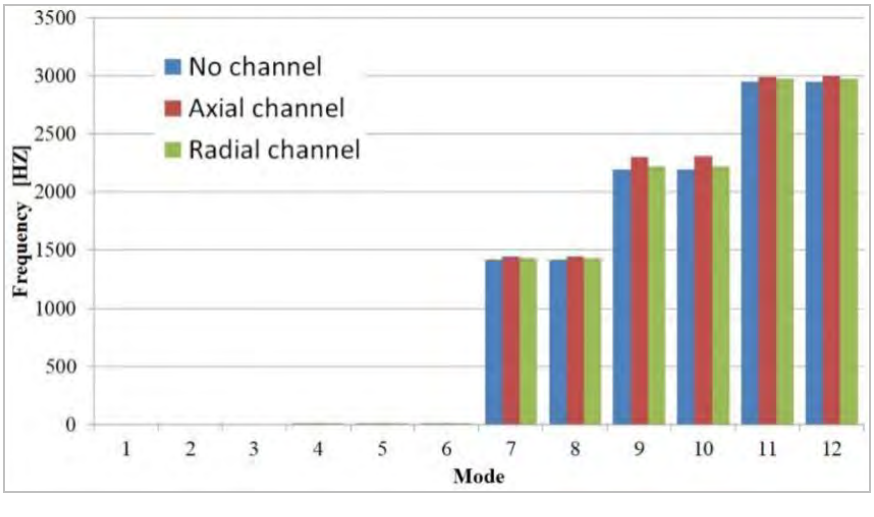

Figure 6 Harmonic response results of three stator structures, (a) harmonic response of stator without heat sink (b) stator harmonic response of radial cooling channel (c) stator harmonic response of axial cooling channel (see online version for colours)

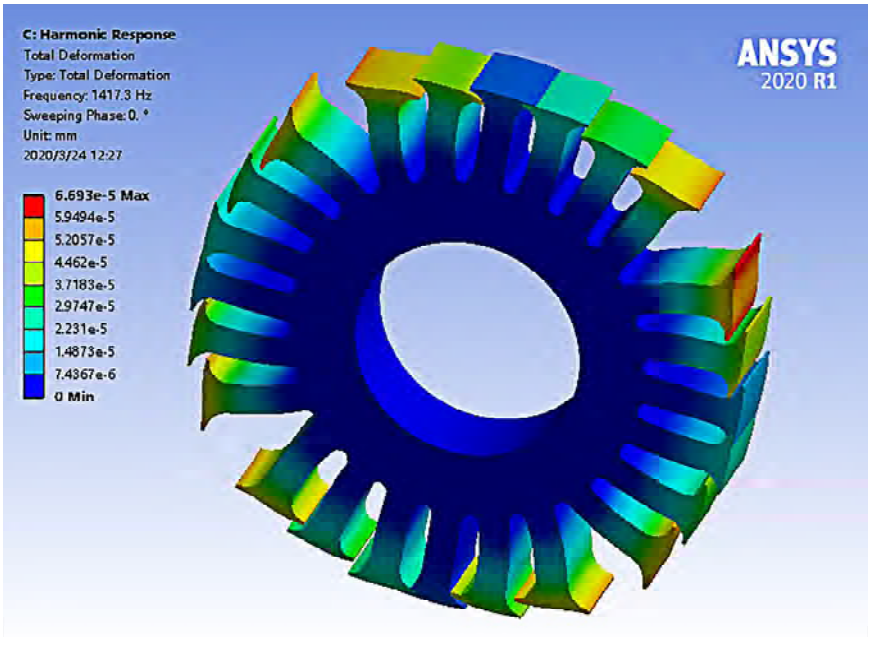

(a)

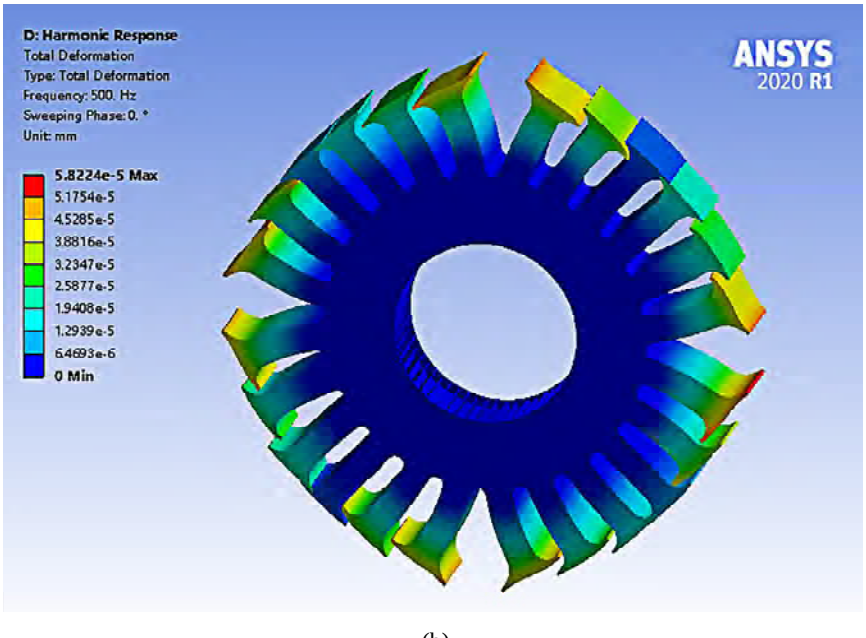

(b)

Figure 6 Harmonic response results of three stator structures, (a) harmonic response of stator without heat sink (b) stator harmonic response of radial cooling channel (c) stator harmonic response of axial cooling channel (continued) (see online version for colours)

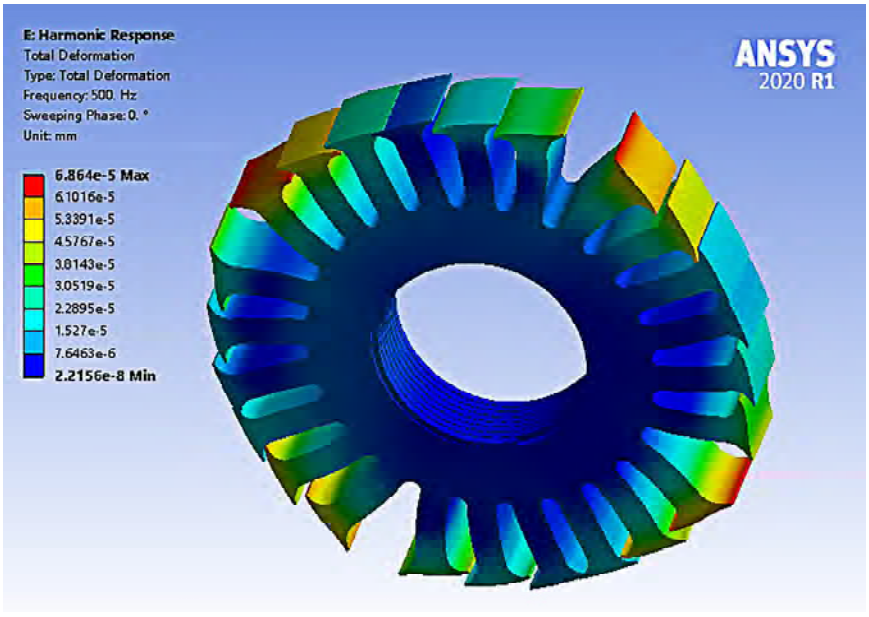

(c)

4 Conclusions and future work

In this paper, the calculation formula of radial force wave of in-wheel motor is deduced, and it is concluded that the radial force wave is the main cause of vibration of in-wheel motor; the radial electromagnetic force wave of in-wheel motor under load is decomposed by Fourier transform, and it is concluded that the radial electromagnetic force wave generated by in-wheel motor has large harmonic amplitude and wide frequency distribution, which is easier to cause resonance of in-wheel motor structure, thus increasing the vibration of in-wheel motor. The results show that the three stator structures of the same order have little influence on the natural frequency, but the natural frequency of the radial channel is slightly higher; under the action of the radial force wave, the maximum deformation of the stator without cooling channel is 6.639e–5 mm, the maximum deformation of the stator with radial cooling channel is 5.8224e–5 mm, and the maximum deformation of the stator with radial cooling channel is 5.8224e–5 mm. The maximum deformation of the stator is 6.864e–5 mm, and its deformation is very small, so there will be no friction and collision between the stator and the rotor during the operation of the in-wheel motor. The following follow-up work:

1 further consider the influence of more complex waterway structure on stator modal and vibration deformation

2 further strengthen the characteristic analysis of electromagnetic noise of in-wheel motor.

Acknowledgements

The authors would like to thank anonymous reviewers for their helpful comments and suggestions to improve the manuscript. This research was supported by the National Natural Science Foundation of China (Grant No. 52162044), the Key Research Program of Jiangxi Province (Grant No. 20212BBE51014), the Nanchang Key Laboratory of Intelligent and Connected New Energy Vehicle (Grant No. 2020-NCZDSY-006) and Jiangxi Province Graduate Innovation Special Fund (YC2021-S461).

References

Chen, Q., Shao, H., Huang, J. et al. (2019) 'Analysis of temperature field and water cooling of outer rotor in wheel motor for electric vehicle', *IEEE Access*, No. 7, pp.140142–140151.

Chen, Q.P., Xie, Y.F., Guo, S.F., Bai, J. and Shu, Q. (2021) 'Sensing system of environmental perception technologies for driverless vehicle: a review of state of the art and challenges', *Sensors and Actuators: A. Physical* Prepublish, Vol. 319, p.112566

Dong, Q., Liu, X., Qi, H. et al. (2019) 'Analysis and evaluation of electromagnetic vibration and noise in permanent magnet synchronous motor with rotor step skewing', *Science China*, Vol. 62, No. 5, pp.133–142.

Gao, P., Sun, X., Tan, S., Zhang, G. Fan. J. and Wang, X. (2019) 'Analysis and optimization of electromagnetic vibration and noise of permanent magnet synchronous motor for electric vehicle', *Micromotor*, Vol. 52, No. 12, pp.7–12.

Hara, T., Ajima, T., Tanabe, Y., Watanabe, M., Hoshino, K. and Oyama, K. (2017) 'Analysis of vibration of permanent magnet synchronous motor with distributed winding for the PWM method of voltage source inverters', *2017 IEEE Energy Conversion Congress and Exposition (ECCE)*.

Jiang, C., Zhou, L., Dong, X., Lu, D. and Jin, L. (2020) 'Finite element analysis and experimental study on radial standing wave ultrasonic motor with large torque', *Vibration and Shock*, Vol. 39, No. 5, pp.57–62+73.

Jing, L. and Cheng, J. (2019) 'Research on torque ripple optimization of switched reluctance motor', *Vibration and Shock*, Vol. 38, No. 21, pp.120–125.

Liang, Y.C., Li, Y.C. and Wang, J.Q. (2014) 'Study on the motor vibration based on LabVIEW and FFT', *Applied Mechanics & Materials*, Vols. 568–570, pp.433–436.

Lin, F., Zuo, S. and Deng, W. (2018) 'Impact of rotor eccentricity on electromagnetic vibration and noise of permanent magnet synchronous motor', *Journal of Vibroengineering*, Vol. 20, No. 2, pp.923–935.

Lin, F., Zuo, S., Deng, W. et al. (2016) 'Modeling and analysis of electromagnetic force, vibration and noise in permanent magnet synchronous motor considering current harmonics', *IEEE Transactions on Industrial Electronics*, Vol. 63, No. 12 pp.7455–7466.

Lu, S., Chen, B., Liu, S. and Jia, W. (2020) 'Research on electromagnetic vibration and noise of induction motor under broken bar state based on multi field coupling', *Large Motor Technology*, Vol. 270, No. 3, pp.17–25.

Pezzaniab, C.M., Bossioab, J.M., Castellinoa, A.M., Bossioab, G.R. and De Angeloab, C.H. (2017) 'A PLL based resampling technique for vibration analysis in variable speed wind turbines with PMSG: a bearing fault case', *Mechanical Systems and Signal Processing*, No. 85, pp.354–366.

Sun, W., Li, Y., Huang, J. et al. (2015) 'Vibration effect and control of in-wheel switched reluctance motor for electric vehicle', *Journal of Sound & Vibration*, Vol. 338, pp.105–120.

Verez, G., Barakat, G., Amara, Y. et al. (2015) 'Impact of pole and slot combination on vibrations and noise of electromagnetic origins in permanent magnet synchronous motors', *IEEE Transactions on Magnetics*, Vol. 51, No. 3, pp.1–4.

Wang, S. and Li, H. (2020) 'Reduction of electromagnetic vibration and noise in permanent magnet motor for EVs by optimizing design of rotor based on GPR PSO model', *Journal of Electrical Engineering & Technology*, Vol. 15, No. 11, pp.1231–1243.

Wang, X. and Qiu, A. (2012) 'Finite element calculation of radial electromagnetic force wave of cage induction motor', *Acta Electrotechnics Sinica*, Vol. 27, No. 7, pp.109–117.

Wang, X., He, X. and Gao, P. (2019) 'Research on electromagnetic vibration and noise reduction method of permanent magnet motor with V shaped magnet rotor for electric vehicle', *Chinese Journal of Electrical Engineering*, Vol. 39, No. 16, pp.281–288+356.

Wu, F.K., Yeh, T.J. and Huang, C.F. (2013) 'Motor control and torque coordination of an electric vehicle actuated by two in wheel motors', *Mechatronics*, Vol. 23, No. 1, pp.46–60.

Zhan, Y., Zhu, H. and Zhou, G. (2019) 'Influence of skewed slot on radial excitation force and vibration of permanent magnet synchronous motor', *Application of Motor and Control*, Vol. 46, No. 5, pp.36–40.

Zhang, J., Lu, J., Yuan, X. et al. (2019) 'Study on vibration and noise of small DC motor based on EMI technology', *Noise and Vibration Control*, Vol. 39, No. 4, pp.134–140.